CrystEngComm

PAPER

View Article Online
View Journal | View Issue

Open Access Article. Published on 26 May 2017. Downloaded on 11/25/2024 5:47:57 AM.
This article is licensed under a Creative Commons Attribution 3.0 Unported Licence.

Check for updates

Cite this: *CrystEngComm*, 2017, **19**, 4933

Modular assembly of porous organic cage crystals: isoreticular quasiracemates and ternary co-crystal†

Srinu Tothadi,[ab] Marc A. Little,[a] Tom Hasell,[a] Michael E. Briggs,[a] Samantha Y. Chong,[a] Ming Liu[a] and Andrew I. Cooper*[a]

Received 25th April 2017,
Accepted 15th May 2017

DOI: 10.1039/c7ce00783c

rsc.li/crystengcomm

Small changes in molecular structure and crystallisation conditions can have a profound effect on the crystal packing of molecules. Increasing the system complexity—for example, by introducing multiple components—greatly increases the number of potential outcomes. Hence, the rational design of porous co-crystals with multiple components is challenging. Here, we report a family of isoreticular quasiracemate crystalline phases for porous organic cages, **FT-RCC3**-*R*·**CC***X*-*S* (where *X* = 1, 2, or 4), that were prepared in a modular and predictable fashion. By using directional intermolecular interactions between cages, we were able to prepare a rare ternary co-crystal, (**CC3**-$S_{0.5}$**CC4**-$S_{0.5}$)·(**CC13**-$S_{0.5}$**CC3**-$S_{0.25}$**CC4**-$S_{0.25}$).

Introduction

Porous organic cages (POCs) are shape persistent molecules with intrinsic cavities that can accommodate guest molecules.[1] Windows in the cage structure allow guest molecules to diffuse into the intrinsic cavities. Hence, organic cages can be crystallised as porous solids,[1] or used to form porous liquids.[2] An increasing number of POC materials have been reported[1,3] with the cage molecules themselves being synthesised *via* imine,[4–8] boronic ester,[9,10] or carbon–carbon[11] bond forming reactions. A diverse series of POCs has now been reported with surface areas as high as 3758 $m^2\ g^{-1}$.[10] Many applications for POCs take advantage of the narrow pore diameter (PD) in these materials,[3] which are typically similar to the size of gases and small molecules. This can impart guest selectivity[12–14] and confinement.[15–17] The accessibility of the intrinsic pore of an isolated cage is dictated by the dimensions of the cage window, but the PD is ultimately determined by how the cages pack in the solid state. Therefore, the function of crystalline POCs is related to the crystal packing of the cages as well as the isolated chemical structure of the cage. Synthetic advances in this field must therefore be coupled with corresponding crystal engineering developments in order to enable real-life applications.

As outlined by Desiraju, there is a lack of generality in the underpinning self-assembly rules for organic crystals.[18] Nevertheless, by using directional bonding interactions, such as halogen and/or hydrogen bonding, it is possible to design modularity in binary and ternary co-crystals.[19–23] However, such complementary directional bonding motifs are not always compatible with cage synthesis. By contrast, there are more generalised strategies for the preparation of framework materials. In multivariate metal–organic frameworks (MOFs),[24,25] ligands with different chemical functionalities can be combined in a modular way within a single porous material. Alternatively, topological blueprints can be used to predict libraries of isoreticular MOFs that can be rationally synthesised.[26] For porous crystalline molecular materials, a

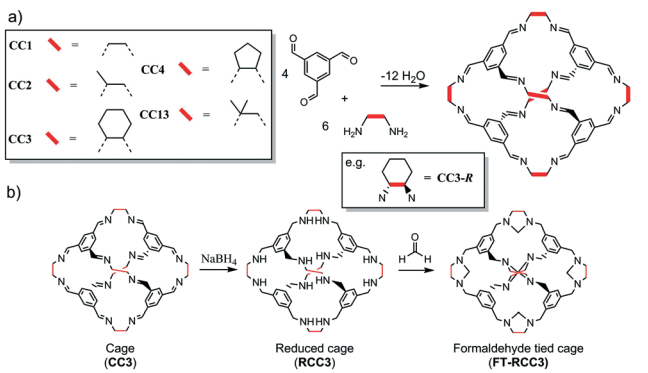

Scheme 1 (a) Shape persistent chiral [4 + 6] imine cages **CC1**–**CC4**, and **CC13**. (b) Transformation of imine cage (**CC3**) to formaldehyde tied cage (**FT-RCC3**).

[a] *Chemistry Department and Materials Innovation Factory, University of Liverpool, Oxford Street, Liverpool, L69 7ZD, UK.*
E-mail: aicooper@liverpool.ac.uk
[b] *Academy of Scientific and Innovative Research Physical/Materials Chemistry Division, CSIR-National Chemical Laboratory, Dr. Homi Bhabha Road, Pune-411008, India*

† Electronic supplementary information (ESI) available. CCDC 1546304 and 1546305. For ESI and crystallographic data in CIF or other electronic format see DOI: 10.1039/c7ce00783c

Open Access Article. Published on 26 May 2017. Downloaded on 11/25/2024 5:47:57 AM.
This article is licensed under a Creative Commons Attribution 3.0 Unported Licence.

parallel strategy does not yet exist, although we have shown that crystal structure prediction has the potential to address this 'design gap'.[27–30] We have also developed a series of design strategies, based on identifying supramolecular interactions, such as chiral recognition[27,28,31] and structure directing guests,[32,33] that allow chemically distinct POCs to be combined as modular building blocks for the predictable assembly of porous crystals.

Here, we report a general strategy for controlling cage–cage co-crystal assembly using chiral recognition, building on our earlier discoveries.[27,31] The molecules used in this study are helically chiral [4 + 6] cycloimine cages (Scheme 1).

The organic cages are formed by reacting 1,3,5-triformylbenzene with different vicinal diamines (Scheme 1a).[4,32,34] For **CC2**, **CC3** and **CC4**, the chirality of the diamine controls the helical chirality of the cage molecule, whereas **CC1** and **CC13** are synthesised using achiral diamines and prepared as helical racemates. For this series of POCs, the intrinsic cage cavity is accessible *via* four chiral triangular windows through which guest diffusion can occur. Subtle differences in the size and shape of the vicinal diamines (vertex groups) has a profound effect on how the cages crystallise as porous solids. For example, **CC3**, which has cyclohexyl vertex groups, typically packs window-to-window (Fig. 1a) and crystallises as a microporous porous solid with an interconnected diamondoid pore channel (**CC3**α, Fig. 1b). Cages **CC1**, **CC2**-*R*, **CC4**-*R*, and **CC13**, which all have similar shaped cores and window dimensions, all pack differently without the use of directing solvents. This is important because the crystal packing of the cages has profound effect on the physical properties. For example, the cavities of all the [4 + 6] cages (Scheme 1) are a near perfect fit for Xe. However, a comparison of the most commonly observed crystal packings for these cages revealed that only **CC3**-*R* crystallised to form a porous solid, **CC3**α, that has additional extrinsic adsorption sites, which are located between the cage windows and are well-matched in size to Xe. This allows **CC3**α to favourably adsorb Xe/Kr with high selectivity and separate Xe from Xe : Kr gas mixtures.[12] We have also shown that **CC3**α can be used to separate xylene mixtures,[35] enantiomers,[12] and hexane isomers.[36] Hence, targeting a series of crystalline phases with this diamondoid pore topology could be advantageous and enable the physical properties of **CC3**α to be varied systematically, as for isoreticular MOFs. Previously, we showed that different cage molecules can be crystallized together to form a single homogeneous structure[27] and that the synthesis of cage–cage co-crystals has tremendous advantages: for example, by providing access to stable crystalline forms.[37] We therefore decided to investigate the crystal packing of two recently discovered cages, **FT-RCC3** (ref. 38) and **CC13**.[32] As individual components, **FT-RCC3** and **CC13** have interesting properties in comparison to our other [4 + 6] cages. For example, **FT-RCC3** is much more stable in acidic and basic solution than **CC3**,[38] and the dimethyl vertices of **CC13** can frustrate the packing of this cage, greatly increasing extrinsic porosity in the crystal structure.[32] Investigating the generality of co-crystal formation with these cages was therefore a desirable target.

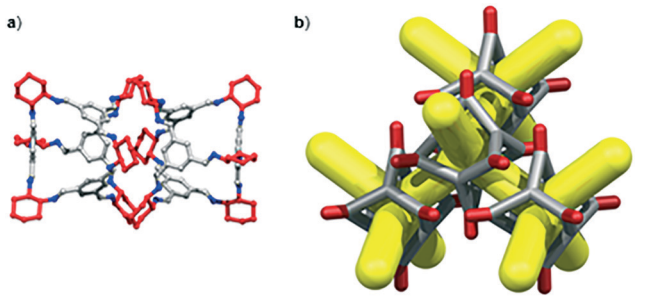

Fig. 1 POC **CC3** packs window-to-window (a) to form a crystalline microporous solid, referred to as **CC3**α, that has a diamondoid shaped pore topology (b).

Experimental

Synthetic procedures

1,3,5-Triformylbenzene was purchased from Manchester Organics, UK. All other chemicals were purchased from Sigma-Aldrich and used as received. The cage molecules **CC1**,[4] **CC2**,[4] **CC3**,[31] **CC4**,[34] **CC13**,[32] and **FT-RCC3** (ref. 38) were synthesised as previously reported. Cage chirality was determined from the synthetic procedures only.

Materials and methods

Single crystal X-ray diffraction (SC-XRD). SC-XRD data was recorded at beamline 11.3.1, Advanced Light Source, Berkeley, USA, using silicon monochromated synchrotron radiation (λ = 0.7749 Å, PHOTON100 CMOS detector); on a Rigaku MicroMax-007 HF rotating anode diffractometer (Mo-Kα radiation, λ = 0.71073 Å, Kappa 4-circle goniometer, Rigaku Saturn724+ detector). Empirical absorption corrections, using the multi-scan method, were performed by the program SADABS.[39] The structures were solved by SHELXT,[40] or by direct methods using SHELXS,[41] and reined by full-matrix least squares refinement on $|F|^2$ by SHELXL,[42] interfaced through the programme OLEX2.[43] Unless stated all non-H atoms were refined anisotropically and were fixed in geometrically estimated positions and refined using the riding model.

Powder X-ray diffraction (PXRD). PXRD data for all single, binary, and ternary crystalline materials were collected in transmission mode on samples held on thin Mylar film in aluminium well plates on a Panalytical X'Pert PRO MPD equipped with a high throughput screening (HTS) XYZ stage, X-ray focusing mirror, and PIXcel detector, using Ni-filtered Cu Kα radiation. Data were measured over the range 5–50° in ~0.013° steps over 60 min. Analysis of the powder diffraction patterns was carried out using *TOPAS-Academic*.[44]

Analytical high-performance liquid chromatography (HPLC). Analytical HPLC analysis was conducted using a Dionex Ultimate 3000 HPLC system. A Thermo Scientific Syncronis C8, 150 × 4.6 mm, 3 μm (97203–154630, 12475)

Open Access Article. Published on 26 May 2017. Downloaded on 11/25/2024 5:47:57 AM.
This article is licensed under a Creative Commons Attribution 3.0 Unported Licence.

column was used for the analysis of all single component cages and co-crystals. The mobile phase was isocratic methanol at a flow rate of 1 mL min^{-1}. The column oven temperature was set to 30 °C. Detection for HPLC analysis was conducted at 254 nm.

Gas sorption analysis. Micromeritics ASAP 2020 volumetric adsorption analyser was used to analyse gas sorption experiments. Surface areas and pore size distributions were measured by nitrogen adsorption and desorption at 77.3 K. Carbon dioxide isotherms were measured at 273 K and 293 K. Xenon and krypton isotherms were measure at 298 K. Samples were degassed offline at 60 °C for 15 hours under dynamic vacuum (10^{-5} bar) before analysis, followed by degassing on the analysis port under vacuum at 80 °C.

Scanning electron microscopy (SEM). High resolution imaging of the crystal morphology was achieved using a Hitachi S-4800 cold Field Emission SEM. Scanning-mode samples were prepared by depositing dry crystals on 15 mm Hitachi M4 aluminium stubs using an adhesive high-purity carbon tab before coating with a 2 nm layer of gold using an Emitech K550X automated sputter coater. Imaging was conducted at a working distance of 8 mm and a working voltage of 3 kV using a mix of upper and lower secondary electron detectors. The field emission SEM measurement scale bar was calibrated using certified SIRA calibration standards.

Electrospray ionization mass spectrometry (ESI-MS). MS was performed using a Finnigan Surveyor MSQ Plus (Thermo Electron Corporation) with methanol as the eluent and 100 V cone voltage, 3.0 kV needle voltage, and +ve ESI.

Thermal gravimetric analysis (TGA). TGA analysis for binary and ternary co-crystal was carried out using a Q5000IR analyser (TA instruments) with an automated vertical overhead thermobalance. Samples were loaded in aluminium pans. The samples were heated at the rate of 10 °C min^{-1}, under nitrogen.

General procedure for preparation of quasiracemate crystalline materials. 4.47 mM stock solutions of the cage molecules **CC1**, **CC2**, **CC3**, **CC4**, **CC13**, and **FT-RCC3** dissolved in dichloromethane (DCM) were prepared. Equal portions of the stock solutions were combined and the targeted cage–cage co-crystals were crystallised from solution using vapour diffusion of acetone. In most cases, the resulting crystalline precipitates were not suitable for SC-XRD and analysis was carried out by PXRD.

Procedure for preparation of ternary co-crystal. Initially, 4.47 mM solutions of the cage molecules **CC3-*S*** (0.5 mL), **CC4-*S*** (0.5 mL), and **CC13** (1 mL) were mixed in 5 mL glass sample vials. Vapour diffusion of acetone into the glass vial afforded octahedral crystals of, (**CC3-$S_{0.5}$CC4-$S_{0.5}$**)·(**CC13-$S_{0.5}$CC3-$S_{0.25}$CC4-$S_{0.25}$**), after five days. After optimization, and for preparation of samples used for gas sorption analysis, **CC3-*S***, **CC4-*S***, and **CC13** were mixed in a 0.375 : 0.375 : 0.25 molar ratio in glass sample vials and vapour diffusion of acetone was carried out for five days. Crystals were collected by filtration and dried under vacuum at 90 °C.

Crystallography refinement details. A single crystal of **FT-CC3-*R*·CC1-*S*** was mounted on MiTeGen gripper and heated to 400 K. After equilibration a full data set was recorded on a Rigaku MicroMax-007 HF rotating anode diffractometer (Mo-Kα radiation, λ = 0.71073 Å, Kappa 4-circle goniometer, Rigaku Saturn724+ detector). Crystal data for **FT-CC3-*R*·CC1-*S***; CCDC # 1546304. Formula $C_{126}H_{156}N_{24}$; M = 2006.75 g mol^{-1}; cubic space group $F23$, colourless prism shape crystal; a = 24.586(3) Å; V = 14 861(5) $Å^3$; ρ = 0.897 g cm^{-3}; μ(Mo-Kα) = 0.054 mm^{-3}; F(000) = 4320; crystal size = 0.17 × 0.15 × 0.09 mm; T = 400(2) K; 26 336 reflections measured ($2.343 < \theta < 20.790°$), 1321 unique (R_{int} = 0.0372), 971 $I > 2\sigma(I)$; R_1 = 0.0491 for the observed and R_1 = 0.0708 for all reflections; wR_2 = 0.1655 for all reflections; max/min residual electron density = 0.119 and −0.064 e $Å^{-3}$; data/restraints/parameters = 1321/67/114; GOF = 1.059.

A single crystal of (**CC3-$S_{0.5}$CC4-$S_{0.5}$**)·(**CC13-$S_{0.5}$CC3-$S_{0.25}$CC4-$S_{0.25}$**) was mounted on MiTeGen gripper and initially heated to 425 K before a data set was recorded at 100 K. Crystal data for (**CC3-$S_{0.5}$CC4-$S_{0.5}$**)·(**CC13-$S_{0.5}$CC3-$S_{0.25}$CC4-$S_{0.25}$**); CCDC # 1546305. Formula = $C_{133.50}H_{176.84}N_{24}O_{11.92}$; M = 2308.50 g mol^{-1}; cubic space group $F23$, colourless prism shape crystal; a = 24.1722(10) Å; V = 14123.7(18) $Å^3$; ρ = 1.086 g cm^{-3}; $\mu(\lambda$ = 0.7749 Å) = 0.085 mm^{-3}; F(000) = 4965; crystal size = 0.2 × 0.19 × 0.15 mm; T = 100(2) K; 32 931 reflections measured ($2.598 < \theta < 28.180°$), 2259 unique (R_{int} = 0.0510), 2031 $I > 2\sigma(I)$; R_1 = 0.0941 for the observed and R_1 = 0.1038 for all reflections; wR_2 = 0.2252 for all reflections; max/min residual electron density = 0.547 and −0.395 e $Å^{-3}$; data/restraints/parameters = 2259/42/203; GOF = 2.259. Due to disorder, during the refinement of (**CC3-$S_{0.5}$CC4-$S_{0.5}$**)·(**CC13-$S_{0.5}$CC3-$S_{0.25}$CC4-$S_{0.25}$**), methyl group C atoms were refined isotropically without riding H atoms.

Results and discussion

We have recently shown that **CC3** can be chemically reduced to afford **RCC3** (Scheme 1b) and that the flexible diamine groups in **RCC3** can be further reacted with formaldehyde to afford the rigid 'tied' cage, **FT-RCC3** (Scheme 1b).[38]

In its native, chirally-pure form, **FT-RCC3**, like the parent cage **CC3**, crystallises in the cubic space group $F4_132$. The cage molecules pack window-to-window, resulting in the formation of a diamondoid shaped pore that runs through the cage cavities. However, the replacement of imine groups in **CC3** with aminal groups in **FT-RCC3** changes the shape of the cage (Fig. 2). From the reported single crystal structures of **CC3** (Fig. 2b),[4] and **FT-RCC3** (Fig. 2c),[38] there is a clear difference in the distance between the centre of the aromatic rings in the cage core; 6.9 Å in **CC3** *versus* 8.3 Å in **FT-RCC3**. Thus, the geometry of the windows is different and the size of the tetrahedron in **FT-RCC3** is 36% larger than in **CC3**. Since the cages pack isostructurally, this results in **FT-RCC3** (a = 25.4857(6) Å) having a larger unit cell edge than **CC3**α (a = 25.016(2) Å) from Le Bail fitted PXRD data.[38] To investigate what effect this might have on the crystallisation properties

Open Access Article. Published on 26 May 2017. Downloaded on 11/25/2024 5:47:57 AM.
This article is licensed under a Creative Commons Attribution 3.0 Unported Licence.

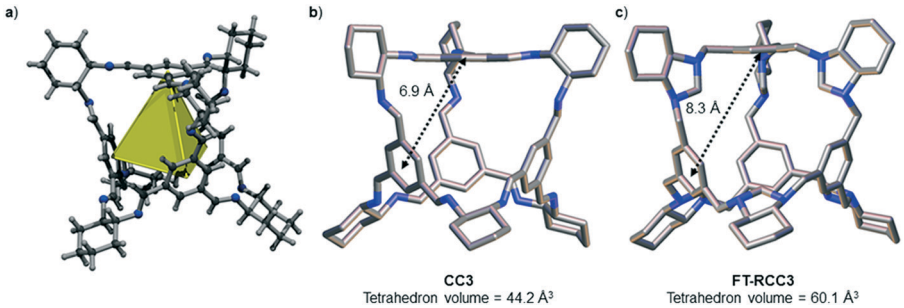

Fig. 2 (a) Structure of [4 + 6] cage molecule highlighting tetrahedral geometry between aromatic groups. From the reported single crystal structures of **CC3** (ref. 4) (b) and **FT-RCC3** (ref. 38) (c) there is a clear difference in the shape and size of the tetrahedral core, resulting in changes to the shape and size of the cage windows. *R* handed cages are shown.

of **FT-RCC3** in comparison to **CC3**, we initially co-crystallised **FT-RCC3**-*R* with racemic **CC1** by combining equal volumes of 4.47 mM stock solutions of **FT-RCC3**-*R* and **CC1** in CH_2Cl_2. Vapour diffusion of acetone into the CH_2Cl_2 solution resulted in the formation of a new quasiracemate, (**FT-RCC3**-*R*)·(**CC1**-*S*), which crystallised in the cubic space group *F*23 as octahedral shaped blocks (Fig. S1†). Although **CC1** is helically chiral, it can readily switch between chiral forms in solution and the solid state.[45,46] Only the comparable -*S* form of **CC1** is found in the crystal structure. We previously observed this behaviour when co-crystallising **CC1** with **CC3**-*R*, whereby preferential heterochiral window-to-window interactions between cage molecules can be energetically more favourable that the comparable homochiral window-to-window interactions. Hence, formation of a racemate or quasiracemate is energetically preferred.[27] This approach is also transferable to macrocycles prepared using chirally pure *trans*-1,2-diaminocyclohexane,[47,48] and trigonal prismatic cages with comparable window dimension to that of **CC3**.[28] As a result of energetically favourable window-to-window interactions, **CC1** self-sorts during crystallisation to enable the exclusive formation of, (**FT-RCC3**-*R*)·(**CC1**-*S*) (Fig. 3). The structure, which crystallised as a solvate, is stable to thermal desolvation of the pores at 400 K, observed while desolvating a single crystal prior to collecting X-ray diffraction data. In the desolvated structure (Fig. 3a) window-to-window packing results in the formation of an interconnected diamondoid pore (Fig. 3b). For further analysis, bulk material was activated by heating crystalline material, collected by filtration, to 90 °C under dynamic vacuum for 12 hours (Fig. 4). TGA also shows that the material is stable to 350 °C (Fig. S2†). It should be noted that for **CC3**, favourable heterochiral window-to-window interactions enables the cages to pack closer together. As a result, the cell parameters determined for racemic **CC3** (ref. 27) (a = 24.639(1) Å) are shorter than those determined for chiral **CC3** (a = 25.016(2) Å). Hence, it is possible to determine the likelihood of two cage molecules crystallising together based upon a shift in the unit cell parameters.

To further explore the generality of our approach, equal volumetric quantities of 4.47 mM solutions of **FT-RCC3**-*R* with **CC2**-*S*, **CC4**-*S*, or **FT-RCC3**-*S* in CH_2Cl_2 were combined. Vapour diffusion of acetone into the CH_2Cl_2 solution resulted in the formation of crystalline powders that we analysed by PXRD. Analysis of the crystallisation screen was carried out by Le Bail fitting the activate PXRD data that was collected at room temperature (Fig. 5).

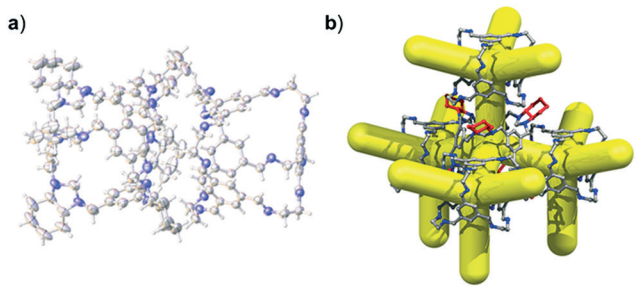

Fig. 3 (a) Desolvated single crystal structure of quasiracemate, (**FT-RCC3**-*R*)·(**CC1**-*S*), showing window-to-window packing between the opposite handed cages. Structure recorded at 400 K; ellipsoids are displayed at 20% probability level. (b) Crystal packing in the single crystal structure, (**FT-RCC3**-*R*)·(**CC1**-*S*), showing interconnected diamondoid pore running through the window-to-window packed cages. **FT-RCC3**-*R* favourably packs window-to-window with **CC1**-*S* in the structure.

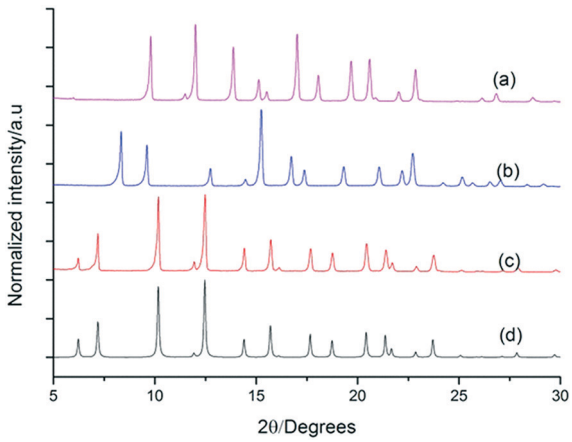

Fig. 4 Experimental PXRD of (a) **FT-RCC3**-*R* (space group symmetry, $F4_132$) (b) racemic **CC1** (*R*3), and (c) activated quasiracemate (**FT-RCC3**-*R*)·(**CC1**-*S*) (*F*23). All crystallised from CH_2Cl_2/acetone. (d) Simulated PXRD of desolvated quasiracemate (**FT-RCC3**-*R*)·(**CC1**-*S*).

 This journal is © The Royal Society of Chemistry 2017

Open Access Article. Published on 26 May 2017. Downloaded on 11/25/2024 5:47:57 AM.
This article is licensed under a Creative Commons Attribution 3.0 Unported Licence.

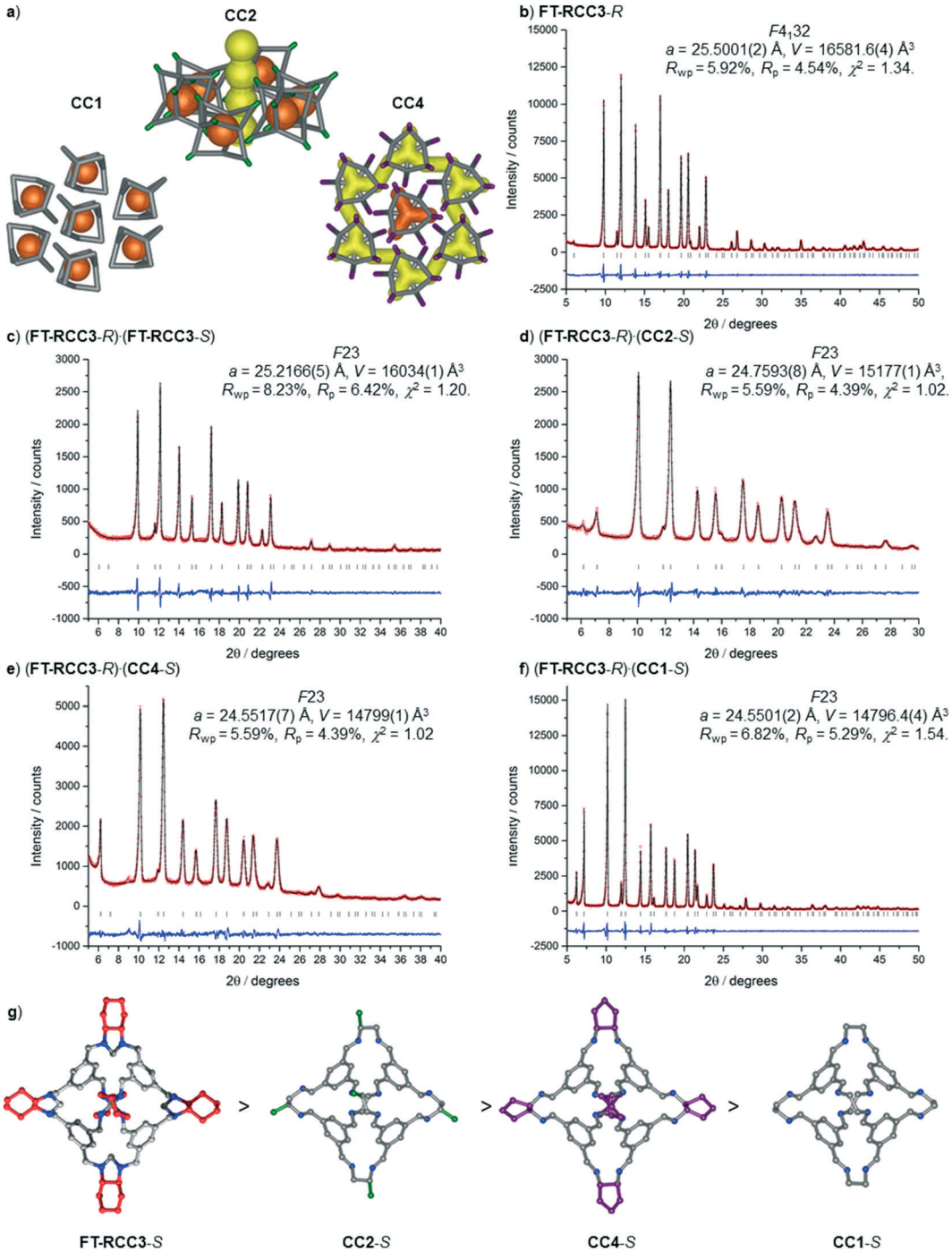

Fig. 5 (a) Graphical representation of pore networks in most commonly observed crystal structures for **CC1**, **CC2**-*R* and **CC4**-*R*. Le Bail fit's for PXRD refined data, (b) **FT-RCC3**-*R*, (c) racemic **FT-RCC3**, (d) (**FT-RCC3**-*R*)·(**CC2**-*S*), (e) (**FT-RCC3**-*R*)·(**CC4**-*S*), and (f) (**FT-RCC3**-*R*)·(**CC1**-*S*); shown in order or decreasing unit cell volume (b → f) that correlates with the trend shown in (g) when these -*S* handed cages are co-crystallised with **FT-RCC3**-*R*.

Analysis of the unit cell parameters determined for the structures revealed a decrease in the unit cell volume along the series **FT-RCC3**-*R* > (**FT-RCC3**-*R*)·(**FT-RCC3**-*S*) > (**FT-RCC3**-*R*)·(**CC2**-*S*) > (**FT-RCC3**-*R*)·(**CC4**-*S*) > (**FT-RCC3**-*R*)·(**CC1**-*S*) (Fig. 5). Importantly, for **CC1**, **CC2**-*S*, and **CC4**-*S*, this also resulted in a change from their typical crystal packing modes (Fig. 5a) when these cages were co-crystallised with **FT-RCC3**-*R*.

To test the solid state porosity of the quasiracemate, (**FT-RCC3**-*R*)·(**CC1**-*S*), a sample was activated and gas sorption analysis was carried out. (**FT-RCC3**-*R*)·(**CC1**-*S*) has a type I N_2 sorption isotherm at 77.3 K with a sharp low pressure step indicative of a microporous material (Fig. 6). (**FT-RCC3**-*R*)·(**CC1**-*S*) adsorbs 4.60 mmol g^{-1} of N_2 at 77.3 K and 1 bar (Fig. 6), and has a calculated apparent Brunauer–Emmett–Teller surface area (SA_{BET}) of 314 m^2 g^{-1}. (**FT-RCC3**-*R*)·(**CC1**-*S*) is also

Open Access Article. Published on 26 May 2017. Downloaded on 11/25/2024 5:47:57 AM.
This article is licensed under a Creative Commons Attribution 3.0 Unported Licence.

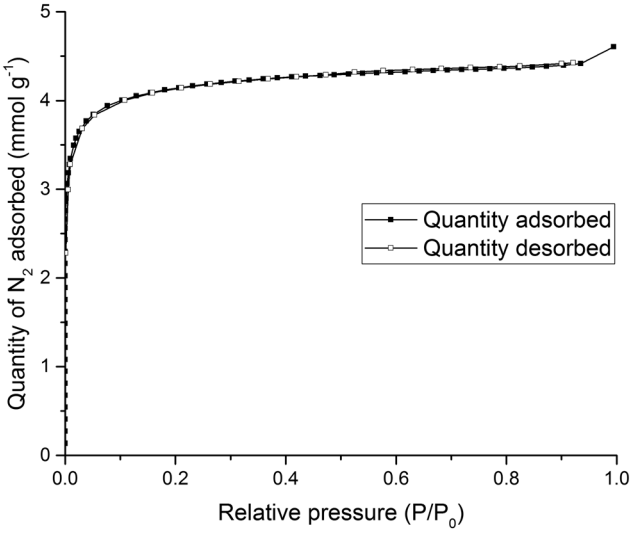

Fig. 6 Type I N_2 gas sorption isotherms for quasiracemate, (**FT-RCC3**-*R*)·(**CC1**-*S*), recorded at 77.3 K.

porous to H_2, CO_2, and CH_4. The material adsorbs 5.23 mmol g^{-1} of H_2 at 77 K and 1 bar (Fig. S3a†), 1.9 mmol g^{-1} of CO_2 at 278 K and 1 bar (Fig. S3b†), and 1.4 mmol g^{-1} of CH_4 at 278 K 1 bar (Fig. S3c†). Importantly, the PXRD of (**FT-RCC3**-*R*)·(**CC1**-*S*) did not change during the gas sorption experiments highlighting that the material did not transform phase during activation and sorption isotherms (Fig. S4†).

It was not possible to isolate a single crystal structure of the quasiracemate, (**FT-RCC3**-*R*)·(**CC13**-*S*), by using comparable crystallisation conditions to those successful for (**FT-RCC3**-*R*)·(**CC1**-*S*). Instead, SC-XRD and PXRD data indicated formation of single component crystals of **FT-RCC3**-*R*, mixed with poorly crystalline **CC13**, when crystallised from CH_2Cl_2/acetone (Fig. S5†). This again highlights the lack of complete generality in designing molecular crystals 'intuitively' when considering the relatively small difference in structure between **CC13** and **CC2** or **CC4**. However, the rational formation of three stable quasiracemate phases in a predictable manner is a further step forward in terms of porous molecular cocrystal design.

Ternary co-crystal

By increasing the number of cage components, a greater number of potential crystallization outcomes are possible. We showed previously that is was possible to form a ternary window-to-window co-crystal comprising the POCs **CC1**, **CC3**-*R*, and **CC4**-*R*,[49] with the general formula, (**CC3**-R_x**CC4**-R_y)·(**CC1**-*S*) (where $x + y = 1$). In the ternary co-crystal, **CC4**-*R* and **CC3**-*R* were disordered over one cage position, as a result, the composition of the ternary co-crystal, and the solid state porosity, could be fine-tuned by varying the molar ratio of **CC3**-*R*:**CC4**-*R* used during crystllisation.[49] To investigate whether **CC13** could also be used to form a ternary co-crystal, we employed the organic cage **CC3**, instead of **FT-RCC3**, because **CC3** and **CC13** are known to cocrystallise.[50] By forming an isoreticular ternary co-crystal, it might follow that a quaternary co-crystal could also be formed, whereby the molar ratio of the cages **CC1** and **CC13** is varied. We therefore initially attempted the ternary co-crystallisation of **CC13** with **CC3**-*S* and **CC4**-*S*. Initially, 1 : 0.5 : 0.5 volumetric ratios of 4.47 mM stock solutions of **CC13**:**CC3**-*S*:**CC4**-*S*, dissolved in CH_2Cl_2, were combined. These ratios were chosen to allow an isostructural ternary co-crystal to be formed. However, slow vapour diffusion of acetone resulted in the formation of prism shaped crystals (Fig. S6†) that were characterised by SC-XRD using synchrotron radiation as, (**CC3**-$S_{0.5}$**CC4**-$S_{0.5}$)·(**CC13**-$S_{0.5}$**CC3**-$S_{0.25}$**CC4**-$S_{0.25}$) (Fig. S7†). This structure, which crystallised in the cubic space group *F*23, has a different cage composition, and crystal structure, to our previously reported ternary co-crystal.[49] Analysis of the structure of the new ternary co-crystal revealed the difference between these phases. In (**CC3**-$S_{0.5}$**CC4**-$S_{0.5}$)·(**CC13**-$S_{0.5}$**CC3**-$S_{0.25}$**CC4**-$S_{0.25}$), **CC3**-*S* and **CC4**-*S* co-crystallise with only the comparable -*S* hand of **CC13**. In addition, the packing of cages is not exclusively window-to-window. In the crystal structure, there are two sites: (**CC3**-$S_{0.5}$**CC4**-$S_{0.5}$) (**site I**); and (**CC13**-$S_{0.5}$**CC3**-$S_{0.25}$**CC4**-$S_{0.25}$) (**site II**) (Fig. 7). **Site I** is shared between **CC3**-*S* and **CC4**-*S* with an approximate 0.5 : 0.5 molar ratio. These cages are superimposed except for the aliphatic rings on the cages

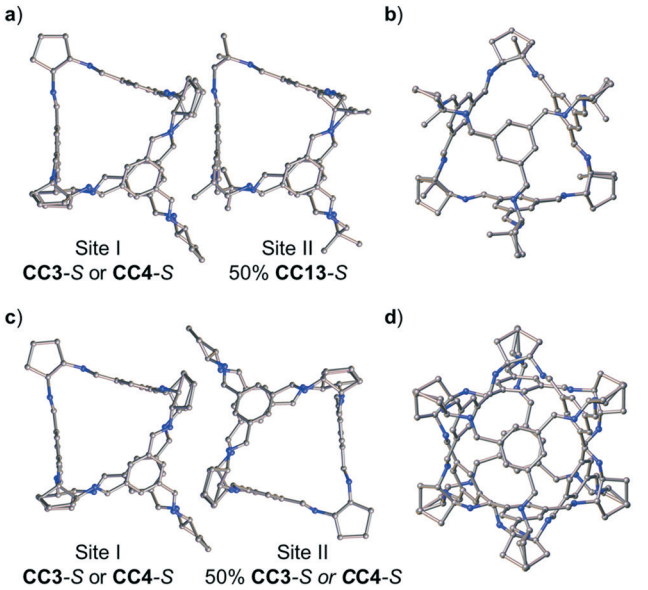

Fig. 7 Crystal packing in co-crystal, (**CC3**-$S_{0.5}$**CC4**-$S_{0.5}$)·(**CC13**-$S_{0.5}$**CC3**-$S_{0.25}$**CC4**-$S_{0.25}$). In the crystal structure the cage molecules are disordered over two sites, **site I** (**CC3**-$S_{0.5}$**CC4**-$S_{0.5}$) and **site II** (**CC13**-$S_{0.5}$**CC3**-$S_{0.25}$**CC4**-$S_{0.25}$). **Site I** is shared between **CC3**-*S* and **CC4**-*S* with an approximate 0.5 : 0.5 molar ratio split. **Site II** is shared between **CC13**-*S*:**CC3**-*S*:**CC4**-*S* with an approximate 0.5 : 0.25 : 0.25 molar ratio split. In approximately 50% of the crystal structure, the **site II** positioned **CC13**-*S* cages are packed window-to-arene with the **site I** positioned **CC4**-*S* or **CC3**-*S* (a and b, two views shown). In the other 50% of the crystal structure the cages are packed window-to-window (c and d, two views shown). **CC3**-*S* and **CC4**-*S* are disordered in the crystal structure and differ only in the size and shape of the cage vertices, only **CC4**-*S* is shown for clarity.

 This journal is © The Royal Society of Chemistry 2017

Open Access Article. Published on 26 May 2017. Downloaded on 11/25/2024 5:47:57 AM.
This article is licensed under a Creative Commons Attribution 3.0 Unported Licence.

vertices, which are chemically different; cyclohexyl rings for **CC3**-*S* *versus* cyclopentyl rings for **CC4**-*S*. **Site II** is shared between **CC13**-*S*, **CC3**-*S*, and **CC4**-*S* with an approximate 0.5 : 0.25 : 0.25 molar ratio split. The -*S* handed form of **CC13**, that occupies 50% of **site II**, is packed window-to-arene with the **CC3**-*S* and **CC4**-*S* molecules positioned on **site I** (Fig. 7a and b). The other 50% of **site II** is occupied by **CC3**-*S* or **CC4**-*S* and these cages pack window-to-window with the **site I** positioned **CC3**-*S* and **CC4**-*S*. Hence, 50% of the crystal structure is window-to-arene packed **CC13**-*S* with **CC3**-*S* or **CC4**-*S*. The other 50% of the crystal structure is window-to-window packed **CC3**-*S* or **CC4**-*S* (Fig. 7c and d).

To evaluate the phase purity and stability of this new ternary co-crystal, which is only the second example reported for POCs, crystals were collected by filtration and characterised by PXRD (Fig. 8). A single phase was determined by PXRD that matches the simulated PXRD pattern of (**CC3**-$S_{0.5}$**CC4**-$S_{0.5}$)·(**CC13**-$S_{0.5}$**CC3**-$S_{0.25}$**CC4**-$S_{0.25}$). TGA also showed that this material was stable up to 375 °C (Fig. S8†).

Due to disorder in the crystal structure, we also carried out qualitative and quantitative HPLC analysis to confirm the exact composition of the ternary co-crystal. The cages have different retention times: **CC3** (7.52 min), **CC4** (6.97 min), **CC13** (4.2 min) (Fig. S9†). Hence, it was possible to accurately determine the cage composition of the disordered ternary co-crystal. To confirm the composition of the new ternary co-crystal before carrying further analysis, a 0.375 : 0.375 : 0.25 molar ratio of **CC3**-*S* : **CC4**-*S* : **CC13**, dissolved in CH_2Cl_2, was combined and crystallised by slow vapour diffusion of acetone. Single crystals were selected using a microscope and dissolved in CH_2Cl_2. HPLC analysis displayed three peaks with retention times of 4.22 min, 6.99 min, and 7.61 min (Fig. S10†). Quantitative analysis of ten different ternary cage co-crystals confirmed the average 0.375 : 0.375 : 0.25 molar ratio between **CC4**-*S* : **CC3**-*S* : **CC13**, in good agreement with the refined crystal structure.

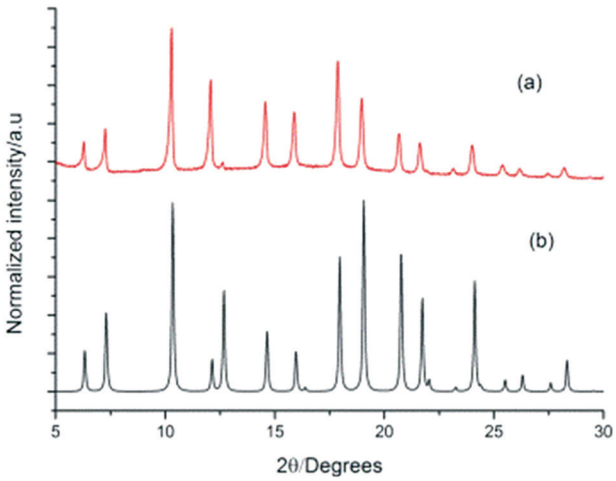

Fig. 8 PXRD of ternary co-crystal, (**CC3**-$S_{0.5}$**CC4**-$S_{0.5}$)·(**CC13**-$S_{0.5}$**CC3**-$S_{0.25}$**CC4**-$S_{0.25}$). (a) Experimental PXRD pattern, and (b) simulated PXRD pattern from single crystal structure. A close match between the patterns is observed.

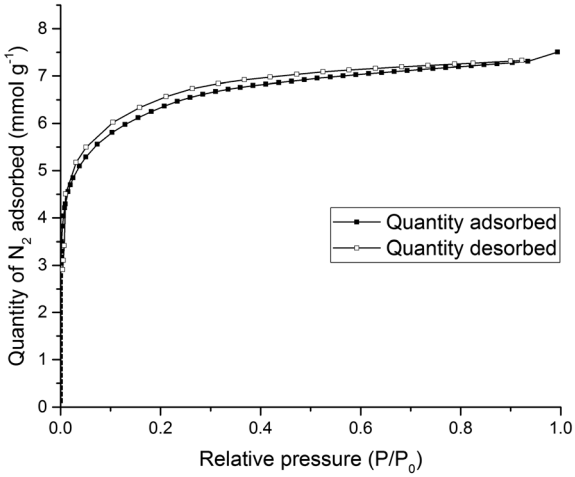

Fig. 9 Type I N_2 gas sorption isotherms for (**CC3**-$S_{0.5}$**CC4**-$S_{0.5}$)·(**CC13**-$S_{0.5}$**CC3**-$S_{0.25}$**CC4**-$S_{0.25}$) recorded at 77.3 K.

To test the porosity of the ternary co-crystal, (**CC3**-$S_{0.5}$**CC4**-$S_{0.5}$)·(**CC13**-$S_{0.5}$**CC3**-$S_{0.25}$**CC4**-$S_{0.25}$) was activated by heating a sample at 90 °C under dynamic vacuum. (**CC3**-$S_{0.5}$**CC4**-$S_{0.5}$)·(**CC13**-$S_{0.5}$**CC3**-$S_{0.25}$**CC4**-$S_{0.25}$) has a type I N_2 sorption isotherm at 77.3 K with a sharp low pressure step (Fig. 9). (**CC3**-$S_{0.5}$**CC4**-$S_{0.5}$)·(**CC13**-$S_{0.5}$**CC3**-$S_{0.25}$**CC4**-$S_{0.25}$) adsorbs 7.51 mmol g^{-1} of N_2 at 1 bar and 77.3 K.

Importantly, the PXRD pattern of (**CC3**-$S_{0.5}$**CC4**-$S_{0.5}$)·(**CC13**-$S_{0.5}$**CC3**-$S_{0.25}$**CC4**-$S_{0.25}$) did not change during sorption analysis indicating that this novel ternary POC co-crystal material was stable during gas sorption analysis (Fig. S12†). (**CC3**-$S_{0.5}$**CC4**-$S_{0.5}$)·(**CC13**-$S_{0.5}$**CC3**-$S_{0.25}$**CC4**-$S_{0.25}$) is also porous to Xe and Kr (Fig. S13†). This indicates that, despite the window-to-arene packing, diffusion of these guests is cooperative. Thus, the material is porous to these gasses even though the window-to-arene packing in 50% of the crystal structure might have resulted in the porosity being 'turned off'.

Conclusions

We have synthesized a family of isoreticular quasiracemates, (**FT-RCC3**-*R*)·(**CCX**-*S*) (where ***X*** = **1**, **2**, or **4**), without the use of strong directional intermolecular bonding interactions. Co-crystallisation is a result of a combination of multiple weak interactions between opposite handed cages. Our results also show that a subtle change in the vertex functionality can increase the number of potential outcomes for the co-crystallisation. This strategy enabled the preparation of a rare ternary co-crystal, (**CC3**-$S_{0.5}$**CC4**-$S_{0.5}$)·(**CC13**-$S_{0.5}$**CC3**-$S_{0.25}$**CC4**-$S_{0.25}$).

Acknowledgements

We thank Rob C. for assistance with gas sorption measurements. We acknowledge the Engineering and Physical Sciences Research Council (EP/N004884/1) and European Research Council under the European Union's Seventh

Open Access Article. Published on 26 May 2017. Downloaded on 11/25/2024 5:47:57 AM.
This article is licensed under a Creative Commons Attribution 3.0 Unported Licence.

Framework Programme (FP/2007-2013) through grant agreement numbers 321156 (ERC-AG-PE5-ROBOT) for funding. T. H. thanks the Royal Society for a University Research Fellowship. We thank the Advanced Light Source, supported by the Director, Office of Science, Office of Basic Energy Sciences, of the US Department of Energy under contract number DE-AC02-05CH11231, and S. J. Teat and K. J. Gagnon for their assistance.

Notes and references

1 T. Hasell and A. I. Cooper, *Nat. Rev. Mater.*, 2016, **1**, 16053.
2 N. Giri, M. G. Del Pópolo, G. Melaugh, R. L. Greenaway, K. Rätzke, T. Koschine, L. Pison, M. F. C. Gomes, A. I. Cooper and S. L. James, *Nature*, 2015, **527**, 216–220.
3 G. Zhang and M. Mastalerz, *Chem. Soc. Rev.*, 2014, **43**, 1934–1947.
4 T. Tozawa, J. T. A. Jones, S. I. Swamy, S. Jiang, D. J. Adams, S. Shakespeare, R. Clowes, D. Bradshaw, T. Hasell, S. Y. Chong, C. Tang, S. Thompson, J. Parker, A. Trewin, J. Bacsa, A. M. Z. Slawin, A. Steiner and A. I. Cooper, *Nat. Mater.*, 2009, **8**, 973–978.
5 M. Mastalerz, M. W. Schneider, I. M. Oppel and O. Presly, *Angew. Chem., Int. Ed.*, 2011, **50**, 1046–1051.
6 Y. Jin, B. A. Voss, R. D. Noble and W. Zhang, *Angew. Chem., Int. Ed.*, 2010, **49**, 6348–6351.
7 S. M. Elbert, F. Rominger and M. Mastalerz, *Chem. – Eur. J.*, 2014, **20**, 16707–16720.
8 M. W. Schneider, H. J. S. Hauswald, R. Stoll and M. Mastalerz, *Chem. Commun.*, 2012, **48**, 9861–9863.
9 G. Zhang, O. Presly, F. White, I. M. Oppel and M. Mastalerz, *Angew. Chem., Int. Ed.*, 2014, **53**, 5126–5130.
10 G. Zhang, O. Presly, F. White, I. M. Oppel and M. Mastalerz, *Angew. Chem., Int. Ed.*, 2014, **53**, 1516–1520.
11 A. Avellaneda, P. Valente, A. Burgun, J. D. Evans, A. W. Markwell-Heys, D. Rankine, D. J. Nielsen, M. R. Hill, C. J. Sumby and C. J. Doonan, *Angew. Chem., Int. Ed.*, 2013, **52**, 3746–3749.
12 L. Chen, P. S. Reiss, S. Y. Chong, D. Holden, K. E. Jelfs, T. Hasell, M. A. Little, A. Kewley, M. E. Briggs, A. Stephenson, K. M. Thomas, J. A. Armstrong, J. Bell, J. Busto, R. Noel, J. Liu, D. M. Strachan, P. K. Thallapally and A. I. Cooper, *Nat. Mater.*, 2014, **13**, 954–960.
13 T. Hasell, M. Miklitz, A. Stephenson, M. A. Little, S. Y. Chong, R. Clowes, L. Chen, D. Holden, G. A. Tribello, K. E. Jelfs and A. I. Cooper, *J. Am. Chem. Soc.*, 2016, **138**, 1653–1659.
14 S.-M. Xie and L.-M. Yuan, *J. Sep. Sci.*, 2017, **40**, 124–137.
15 R. McCaffrey, H. Long, Y. Jin, A. Sanders, W. Park and W. Zhang, *J. Am. Chem. Soc.*, 2014, **136**, 1782–1785.
16 B. Mondal, K. Acharyya, P. Howlader and P. S. Mukherjee, *J. Am. Chem. Soc.*, 2016, **138**, 1709–1716.
17 M. Liu, L. Chen, S. Lewis, S. Y. Chong, M. A. Little, T. Hasell, I. M. Aldous, C. M. Brown, M. W. Smith, C. A. Morrison, L. J. Hardwick and A. I. Cooper, *Nat. Commun.*, 2016, **7**, 12750.
18 G. R. Desiraju, *Angew. Chem., Int. Ed.*, 2014, **53**, 1516–1520 (*Angew. Chem., Int. Ed. Engl.*, 1995, **34**, 2311–2327).
19 C. B. Aakeroy and D. J. Salmon, *CrystEngComm*, 2005, **7**, 439–448.
20 S. Tothadi and G. R. Desiraju, *Chem. Commun.*, 2013, **49**, 7791–7793.
21 F. Topić and K. Rissanen, *J. Am. Chem. Soc.*, 2016, **138**, 6610–6616.
22 A. S. Sinha and C. B. Aakeröy, in *Reference Module in Chemistry, Molecular Sciences and Chemical Engineering*, Elsevier, 2016, DOI: 10.1016/B978-0-12-409547-2.13696-0.
23 S. Tothadi, P. Sanphui and G. R. Desiraju, *Cryst. Growth Des.*, 2014, **14**, 5293–5302.
24 H. Deng, C. J. Doonan, H. Furukawa, R. B. Ferreira, J. Towne, C. B. Knobler, B. Wang and O. M. Yaghi, *Science*, 2010, **327**, 846–850.
25 H. Furukawa, K. E. Cordova, M. O'Keeffe and O. M. Yaghi, *Science*, 2013, **341**, 1230444.
26 D. A. Gomez-Gualdron, Y. J. Colon, X. Zhang, T. C. Wang, Y.-S. Chen, J. T. Hupp, T. Yildirim, O. K. Farha, J. Zhang and R. Q. Snurr, *Energy Environ. Sci.*, 2016, **9**, 3279–3289.
27 J. T. A. Jones, T. Hasell, X. Wu, J. Bacsa, K. E. Jelfs, M. Schmidtmann, S. Y. Chong, D. J. Adams, A. Trewin, F. Schiffman, F. Cora, B. Slater, A. Steiner, G. M. Day and A. I. Cooper, *Nature*, 2011, **474**, 367–371.
28 A. G. Slater, M. A. Little, A. Pulido, S. Y. Chong, D. Holden, L. Chen, C. Morgan, X. Wu, G. Cheng, R. Clowes, M. E. Briggs, T. Hasell, K. E. Jelfs, G. M. Day and A. I. Cooper, *Nat. Chem.*, 2017, **9**, 17–25.
29 E. O. Pyzer-Knapp, H. P. G. Thompson, F. Schiffmann, K. E. Jelfs, A. I. Cooper and G. M. Day, *Chem. Sci.*, 2014, **5**, 2235–2245.
30 A. Pulido, L. Chen, T. Kaczorowski, D. Holden, M. A. Little, S. Y. Chong, B. J. Slater, D. P. McMahon, B. Bonillo, C. J. Stackhouse, A. Stephenson, C. M. Kane, R. Clowes, T. Hasell, A. I. Cooper and G. M. Day, *Nature*, 2017, **543**, 657–664.
31 T. Hasell, S. Y. Chong, K. E. Jelfs, D. J. Adams and A. I. Cooper, *J. Am. Chem. Soc.*, 2012, **134**, 588–598.
32 T. Hasell, J. L. Culshaw, S. Y. Chong, M. Schmidtmann, M. A. Little, K. E. Jelfs, E. O. Pyzer-Knapp, H. Shepherd, D. J. Adams, G. M. Day and A. I. Cooper, *J. Am. Chem. Soc.*, 2014, **136**, 1438–1448.
33 M. A. Little, S. Y. Chong, M. Schmidtmann, T. Hasell and A. I. Cooper, *Chem. Commun.*, 2014, **50**, 9465–9468.
34 T. Mitra, X. Wu, R. Clowes, J. T. A. Jones, K. E. Jelfs, D. J. Adams, A. Trewin, J. Bacsa, A. Steiner and A. I. Cooper, *Chem. – Eur. J.*, 2011, **17**, 10235–10240.
35 T. Mitra, K. E. Jelfs, M. Schmidtmann, A. Ahmed, S. Y. Chong, D. J. Adams and A. I. Cooper, *Nat. Chem.*, 2013, **5**, 276–281.
36 A. Kewley, A. Stephenson, L. Chen, M. E. Briggs, T. Hasell and A. I. Cooper, *Chem. Mater.*, 2015, **27**, 3207–3210.
37 M. A. Little, M. E. Briggs, T. A. JonesJames, M. Schmidtmann, T. Hasell, S. Y. Chong, K. E. Jelfs, L. Chen and A. I. Cooper, *Nat. Chem.*, 2015, **7**, 153–159.

 This journal is © The Royal Society of Chemistry 2017

Open Access Article. Published on 26 May 2017. Downloaded on 11/25/2024 5:47:57 AM.
This article is licensed under a Creative Commons Attribution 3.0 Unported Licence.

38 M. Liu, M. A. Little, K. E. Jelfs, J. T. A. Jones, M. Schmidtmann, S. Y. Chong, T. Hasell and A. I. Cooper, *J. Am. Chem. Soc.*, 2014, **136**, 7583–7586.
39 G. M. Sheldrick, *SADABS*, University of Göttingen, Germany, 2008.
40 G. M. Sheldrick, *Acta Crystallogr., Sect. A: Found. Adv.*, 2015, **71**, 3–8.
41 G. M. Sheldrick, *Acta Crystallogr., Sect. A: Found. Crystallogr.*, 2008, **64**, 112–122.
42 G. Sheldrick, *Acta Crystallogr., Sect. C: Struct. Chem.*, 2015, **71**, 3–8.
43 O. V. Dolomanov, L. J. Bourhis, R. J. Gildea, J. A. K. Howard and H. Puschmann, *J. Appl. Crystallogr.*, 2009, **42**, 339–341.
44 *TOPAS-Academic v. 5 Coelho Software*, Brisbane, Australia, 2012.
45 K. E. Jelfs, F. Schiffmann, J. T. A. Jones, B. Slater, F. Cora and A. I. Cooper, *Phys. Chem. Chem. Phys.*, 2011, **13**, 20081–20085.
46 J. T. A. Jones, D. Holden, T. Mitra, T. Hasell, D. J. Adams, K. E. Jelfs, A. Trewin, D. J. Willock, G. M. Day, J. Bacsa, A. Steiner and A. I. Cooper, *Angew. Chem., Int. Ed.*, 2011, **50**, 749–753.
47 Z. Liu, J. Sun, Y. Zhou, Y. Zhang, Y. Wu, S. K. M. Nalluri, Y. Wang, A. Samanta, C. A. Mirkin, G. C. Schatz and J. F. Stoddart, *J. Org. Chem.*, 2016, **81**, 2581–2588.
48 Y. Wu, S. K. M. Nalluri, R. M. Young, M. D. Krzyaniak, E. A. Margulies, J. F. Stoddart and M. R. Wasielewski, *Angew. Chem., Int. Ed.*, 2015, **54**, 11971–11977.
49 T. Hasell, S. Y. Chong, M. Schmidtmann, D. J. Adams and A. I. Cooper, *Angew. Chem., Int. Ed.*, 2012, **51**, 7154–7157.
50 T. Hasell, M. A. Little, S. Y. Chong, M. Schmidtmann, M. E. Briggs, V. Santolini, K. E. Jelfs and A. I. Cooper, *Nanoscale*, 2017, DOI: 10.1039/c7nr01301a.